Generating turbulence in Wind tunnel experiments: use of passive grids[1]

Giulio Vita[2]

Abstract. Grid generated turbulence is the easiest way of varying the turbulent fluctuations at the inlet of any wind tunnel test. Nevertheless, only few examples in the literature have tried to vary independently turbulence intensity, I, and integral length scale of turbulence, L, posing a challenging interpretation for the assumed effect of turbulence on bluff body aerodynamics. In this study a set of grid is sized according to well-accepted results of the literature and then tested to vary I and L accordingly. The results show an acceptable degree of isotropy and the possibility of obtaining L up to 30cm while having a range of I varying from 15% to 5%.

[1] This is the final report of the Short-Term Scientific Mission (STSM), COST-STSM-TU1304-35490, within the TU1304 WINERCOST Action, carried out by Giulio Vita, from the University of Birmingham, who visited the Aerolasticity and Experimental Aerodynamics Lab, Department of Aerospace and Mechanical Engineering, of the University of Liège, from 13th to 24th of February 2016.

[2] Department of Civil Engineering, School of Engineering, University of Birmingham, B15 2TT, Edgbaston, Birmingham, United Kingdom. e-mail: g.vita@bham.ac.uk

Table of Contents

1. Background

1.1. Participants of the Short Term Scientific Mission

This Scientific Mission was pursued by Giulio Vita, Ph.D. Student from the Department of Civil Engineering of the School of Engineering, at the University of Birmingham, United Kingdom. The supervisors are Dr Hassan Hemida and Prof Charalampos Baniotopoulos from the same Institution.

1.2. Host Institution

The Mission took place at the Aeroelasticity and Experimental Aerodynamics Lab of the Department of Aerospace and Mechanical Engineering of the University of Liège, Belgium, under the supervision of the Head of the Lab, Dr Thomas Andrianne.

1.3. Mission & Timing

The main aim of the STSM was to conduct wind tunnel experiments to design a turbulent inlet capable of varying turbulence intensity and length scale independently. The purpose of such a study is to later investigate the effect of turbulence on bluff body aerodynamics. This was obtained through following objectives:

1. A comprehensive literature review on passive grid generated turbulence.
2. Individuation of suitable set of grids and distances.
3. Measurement of velocity at multiple heights to check uniformity.
4. Post-processing of velocity signal to plot the turbulence statistics.

The experimental setup was also tuned in order to place a bluff body specimen to provide controlled statistics of turbulence at the inlet. This research is aimed to help gain further insight on the complex mechanisms influencing the interaction of free stream turbulence, which is found in atmospheric boundary layer flows, and the aerodynamic performance of bluff bodies.
The Mission started on the 13th of February and ended on the 24th of February 2017.

Table 1 – Timing of the Short Term Scientific Mission

Day	Activity
13 Feb 2017	Arrival at the University of Liège
14 Feb 2017	Visit of the Aeroelasticity and experimental aerodynamics lab. Assessment of the work schedule and statement of limitation due to wind tunnel setup.
15 Feb 2017	Comprehensive literature review of passive grids and empirical relations.
16 Feb 2017	Preliminary design of grid.
17 Feb 2017	Construction of set of 4 grids and setup in the wind tunnel.
18 Feb 2017	Setup of Cobra Probe and first preliminary measurements.
19 Feb 2017	Measurements for grid #1 and #2 and 3 positions.
20 Feb 2017	Measurements for grid #1 and #2 and remaining 2 positions.
21 Feb 2017	Measurements for grid #3 and #4 and 4 positions.
22 Feb 2017	Post-processing of raw data in MatLab
23 Feb 2017	Post-processing of raw data in MatLab and discussion of results.
24 Feb 2017	Presentation of work at the Department of Aerospace and Mechanical Engineering. Departure from the University of Liège

2. Design of the experiment

Generation of inlet turbulence, or rather Free Stream Turbulence, FST, in Wind Tunnel Experiments, can be obtained following several methodologies (Hinze, 1975). Grid generation is accounted as the most effective and reliable source of producing an isotropic field of turbulence at the inlet of experiments (Roach, 1987).
In the following, a discussion about the choice of the proper turbulence generation technique of this study will be given. A further explanation on the choice of the experimental setup and the design of the turbulence generator is also given.

2.1. Literature review

Among the numerous techniques which have been attempted to vary the levels of turbulence (either to damp it either to increase it) at the inlet of wind tunnels, grid generation is the most popular. This is obviously related to the intrinsic simplicity of the experimental setup. However, several limitations exist, which must be valued accurately to assess the goodness of the created flow field.

Active grids

One typology of turbulence generator is the so-called active grid (AG). A number of winglets mounted on a series of shafts are made rotating to generate a turbulent isotropic flow downstream to the grid (Makita, 1991; Makita and Sassa, 1991). The constructive aspects of an active grid have been further perfected (Brzek et al., 2009; Cal et al., 2010). The flow features show that an integral length scale, which is larger than the mesh size, and high turbulent Reynolds numbers (based on Taylor micro-scales) are obtainable (Mydlarski and Warhaft, 2006). The turbulence characteristics can be modelled and fine-tuned by acting on the rotating speed of the winglet-shafts (Cekli and van de Water, 2010; Kang et al., 2003). This method has also been used effectively in a number of works about the effect of turbulence on aerofoils (Maldonado et al., 2015). However, the complicated and expensive setup and the implicit difficulty in fine-tuning the setting of the winglets, together with a paucity in the general number of applications, suggests that a simpler approach is more suitable for the purpose of this report.

Passive grids

The most common typology of turbulence generation is the use of a passive grid (PG) at the inlet-nozzle of wind tunnels. The generation of vorticity due to the presence of the grid and the consequent drop in the pressure field cause the quiescent upstream flow to have well-known characteristics. The flow undergoes a series of transitions. (i) Vortices are shed downstream the bars of the grid, rapidly evolving to form a (ii) field of fully developed turbulence. The turbulent field is then affected by the decay of turbulence, and (iii) slow rotating vortices are finally dominating the turbulence features (Batchelor, 1965). This behaviour is common to the various typologies of grids, reported in the literature (Roach, 1987):

(i) Square mesh arrays of circular rods;
(ii) Square mesh arrays of square bars;
(iii) Parallel arrays of circular rods;
(iv) Parallel arrays of square bars;
(v) Perforated plates, with a variety of configurations.

For a careful review of the behaviour of the flow downstream of a grid, much information can be found in the literature (Batchelor, 1953; Bearman and Morel, 1983; Hinze, 1975; Nakamura, 1993; Nakamura et al., 1988; Roach, 1987). Albeit the intrinsic simplicity of this kind of flow, several and sometimes conflicting opinions are found in the literature regarding an optimal setup to obtain a fully

turbulent isotropic flow field at the inlet of a wind tunnel experiment. Comte-Bellot and Corrsin (1966) pointed out the necessity of adjusting the anisotropy of the flow which occurs due to the blockage effect of the grid, and many authors follow this suggestion in their experimental setup (Bereketab et al., 2000; Mish and Devenport, 2006; Swalwell et al., 2004; Wang et al., 2014). However, this anisotropy seems to depend more on the used measurement equipment, as Roach (1987) showed that grid turbulence is, in fact, much more isotropic than believed.

A wide range of materials, sizes and shapes for the bars composing the grid is found in the literature. It has been argued that circular rods show a dependency on the Reynolds number, unlike square bars. This occurs because of the effects on the separation length and the wake pattern of cylinders for a given flow and material (Bearman and Morel, 1983). As squares feature a determined separation at the blunt corners, the variability of their wakes is limited: studies which imply a variation of the velocity of the flow would benefit square bars to limit the variability of the turbulent field. Smoothing or trimming the corners of such bars has already been found having a limited impact in the turbulence characteristics downstream the grid (Nakamura et al., 1988).

If a square section is chosen for the bars, the grid can still be built in several ways:

(i) Bi-planar grid (two sets of parallel bars placed side-by-side);
(ii) Mono-planar grid (two set of overlapping parallel bars);
(iii) A single set of parallel bars, either vertical or horizontal.

These details do not play a significant role, if the distance between the grid and the object is adjusted to consider $x/M>10$, i.e. until the flow is fully developed. This suggests the need to check the flow statistics if a different range is used, as the limit $x/M>5$ appears more suitable for achieving sufficiently high turbulence intensities. Bearman and Morel (1983) pointed out that the mean velocity downstream to the grid is non-uniform, because of the influence of the wakes of the bars. This non-uniformity decays much faster than that of the turbulence intensity for a mono-planar grid. This behaviour is accounted as true if the solidity of the grid, defined as the ratio between obstruction of bars and opening of the mesh, is kept limited. A high solidity grid is then not advised, and therefore in this work the porosity β of the grid, is limited to the 50%.

$$\beta=(1-b/M)^2>0.5$$

where b is the width of the bars and M is the dimension of the mesh, i.e. the distance between bars.

2.2. Grid generated turbulence

Roach (1987) provided a comparison in the behaviour of different grid generators, presenting several convenient relations to describe the trend of the turbulence characteristics in the fully developed region of the flow downstream the grid. It is meaningful, that the only geometrical parameter, which affects the behaviour, is the width b of the bars, being the mesh size M important to understand the role of the distance at which the flow is truly developed.

Grid generated turbulence intensity decays with downstream distance with an exponential rate. The most trusted exponent given in the literature is -5/7 (Roach, 1987) or -8/9 (Laneville et al., 1975). This expression fits better on bar size rather than mesh. It is also stressed that to evaluate isotropy, turbulence intensity measurements can be misleading, as a simplistic interpretation might suggest a strong anisotropy, which is not the case as found out by Roach (1987). In fact, the analysis of the power spectra and correlation measurements bend towards a more isotropic behaviour of turbulence. Besides the ease of fitting Karman's one-dimensional spectrum to the data, it is also agreed that integral length scale is rather independent of the typology of grid and correlates to the bar size. Micro-scales show a strong dependence on Reynolds, while indicating a strong rate of isotropy for all grids.

A set of empirical constants, varying with the typology of bars, is found to fit the numerous experimental data (Table 2).

Table 2 – Empirical relations for turbulence characteristics

	Longitudinal Turb. Intensity	Transversal Turb. Intensity	Integral Longitudinal Length Scale	Taylor's micro-scale
Parameter	$I_u=\sqrt{\overline{u'^2}}/\bar{u}$	$I_v=\sqrt{\overline{v'^2}}/\bar{u}$	$L_x=\bar{u}\int_0^\infty R_{uu}(\tau)d\tau = =\left[E(n)\bar{u}/\left(4\overline{u'^2}\right)\right]_{n\to 0}$	$\frac{1}{\lambda_x^2}=\frac{2\pi^2}{U^2\overline{u'^2}}\int n^2E_u\,dn$
Empirical expression	$I_u=A(x/b)^{-5/7}$	$I_v=AB(x/b)^{-5/7}$	$L_x/b=C(x/b)^{1/2}$	$\left(\frac{\lambda_x}{b}\right)^2=\frac{14F(x/b)}{Re_b}$
Constants	$A=1.13$	$B=0.89$	$C=0.20$	$F=1.21$

To better understand the performance of the proposed empirical formulas, several results found in the literature, from a variety of fields, have been plotted together to understand the possibility of predicting the turbulence statistics for a given grid make (Bearman and Morel, 1983; Laneville, 1990, 1973; Lee, 1975; Mannini et al., 2017; MCLAREN et al., 1969; MULHEARN, 1973; Nakamura, 1993; Sicot et al., 2008; Swalwell, 2005). In Fig. 1 an overview of the turbulence intensity and the integral length scale of turbulence is proposed. The results are associated by the typology of the grid used: a square bar mono- or bi-planar passive grid.

It is first noticeable that the accuracy of the empirical formulas is extremely variable with the specific set or experimental facility. However, except for the experiment of Swalwell (2005), which used a contraction to help having an isotropic turbulence characteristics, as suggested by Comte-Bellot and Corrsin (1966), the expected behaviour of turbulence with distance is captured with sufficient accuracy for turbulence intensity, while for turbulent length scale the make of the grid has a more important effect. Also, results by Sicot et al. (2008) confirm the crucial importance of the design of the grid and the validation of the obtained turbulence field.

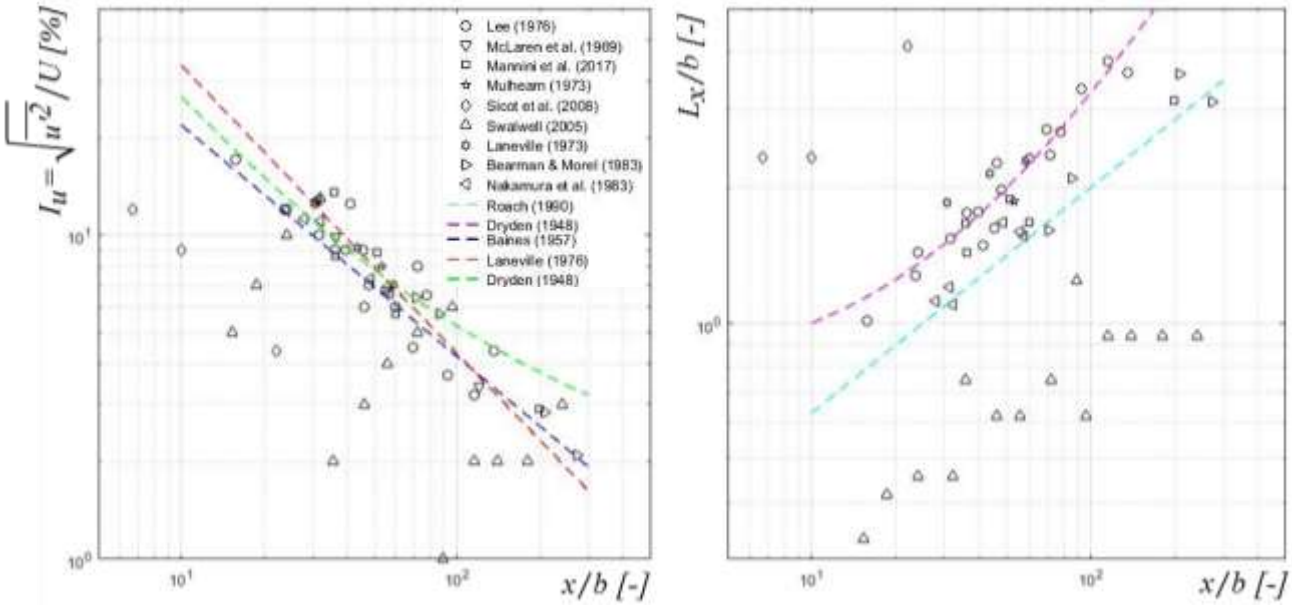

Fig. 1 -

Fig.1 also confirms the validity of the limitations to the porosity $\beta \geq 0.5$ which have therefore been respected in designing the experiment. The empirical formulas used here have been found in the literature and the ones proposed by Roach (1987) enjoy widespread acceptance. However, it is noticeable that a truly careful assessment of the turbulent field is necessary to trustfully use the turbulent grid inlet for applied uses.

2.3. Estimation of turbulence statistics

The design of this experiment involves primarily the choice of the wanted turbulence field. Following this approach, several ratios of distances and grid sizes have been attempted to obtain truly variable turbulence statistics. The relation between the turbulence field and the grid make has been taken from the previously presented empirical formulas (cfr. Section 2.2).

In particular, the bar size b is considered as the lead parameter, as the mesh size is chosen according to acceptable values of the porosity $\beta \geq 0.5$.

The aim for this experiment is to produce a suitable turbulence field, which will allow to variate turbulence intensity and integral length scale separately, with the latter being larger than what is normally available in traditional wind tunnel testing L_x*~25-30cm*. Another requirement of the experiment is to produce Reynolds independent turbulence statistics. As the effect of turbulence might be an effect of the relative size of the eddies with respect of the studied bluff body, then it is useful to adjust the Reynolds range for the body without changing the turbulence statistics. Therefore the chosen grid typology needs to have Reynold independent characteristics. Therefore, the passive square bi-planar grid (ii) is chosen (Roach, 1987).

A variation of bar and mesh sizes has then been attempted to find the best possible combination to obtain truly variable statistics. To aid the choice, Length scales have been plotted against turbulence intensities (Fig. 2). Being the bar sizes limited to the available sizes on the market, the mesh size have been varied accordingly. An optimal ratio of M/b *=3.5-4.5* has been chosen for the parametric study. In Fig. 2 the best combinations are shown for grid #1-3. Grid #4 has been introduced later to amend the actual measured turbulence field.

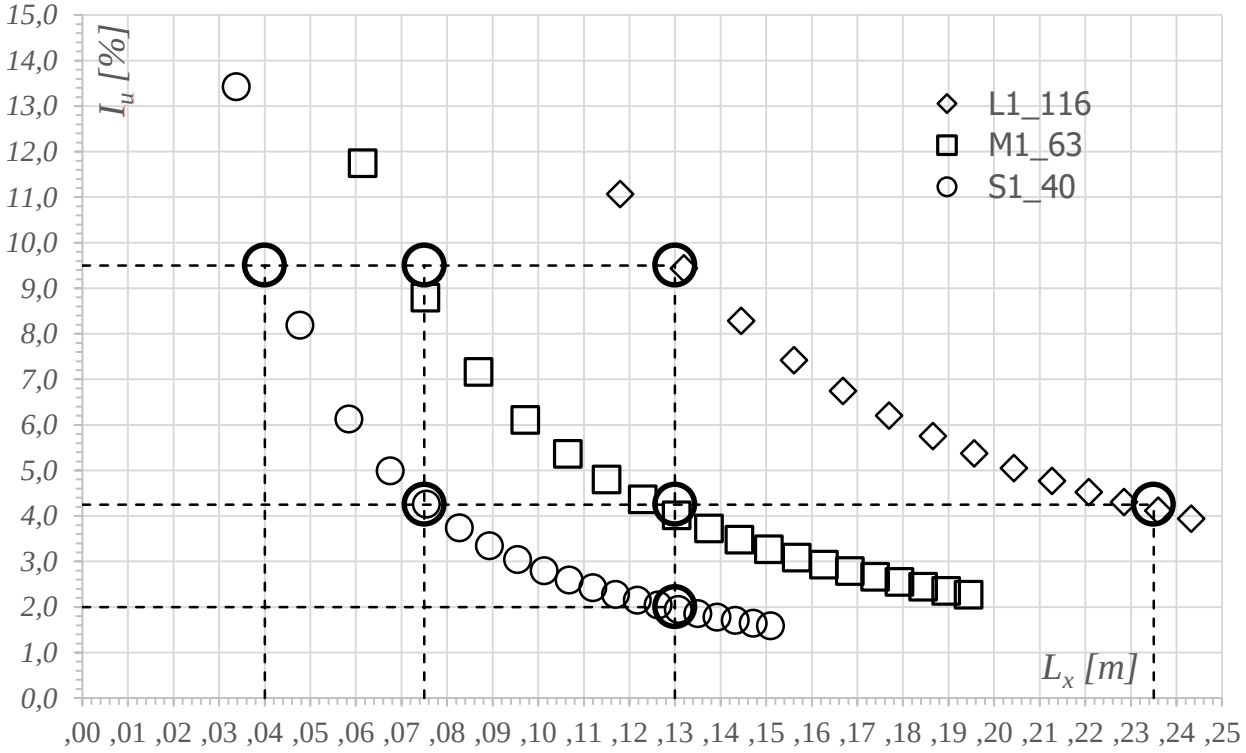

Fig. 2 –

3. *Experimental setup*

In this experiment the passive grid, PG, simple biplanar square grid is put at the inlet nozzle of the test section, without the use of any down-stream contraction. The closed loop wind tunnel of the University of Liège provides the optimal setup for the experiment due to its large size of its cross-section *1.50×1.80* and its length *>15m*. The wooden square bars have been overlapped in a bi-planar mesh to construct the set of grids, which have been placed as needed at the inlet nozzle of the wind tunnel using an aluminium frame firmly fixed to the steel walls of the tunnel.

The turbulence field has been assessed in 5 positions, which have been chosen depending on the mesh size for the various grids $x/M>5\text{-}10$. Fig. 3 shows the experimental setup. As it can be noticed an expansion downstream the grid is present. This connect the small Test Section 1 with the wind tunnel boundary layer test section 2 *2.00×2.50*. This has some effect in the results, as shown in Section 4.

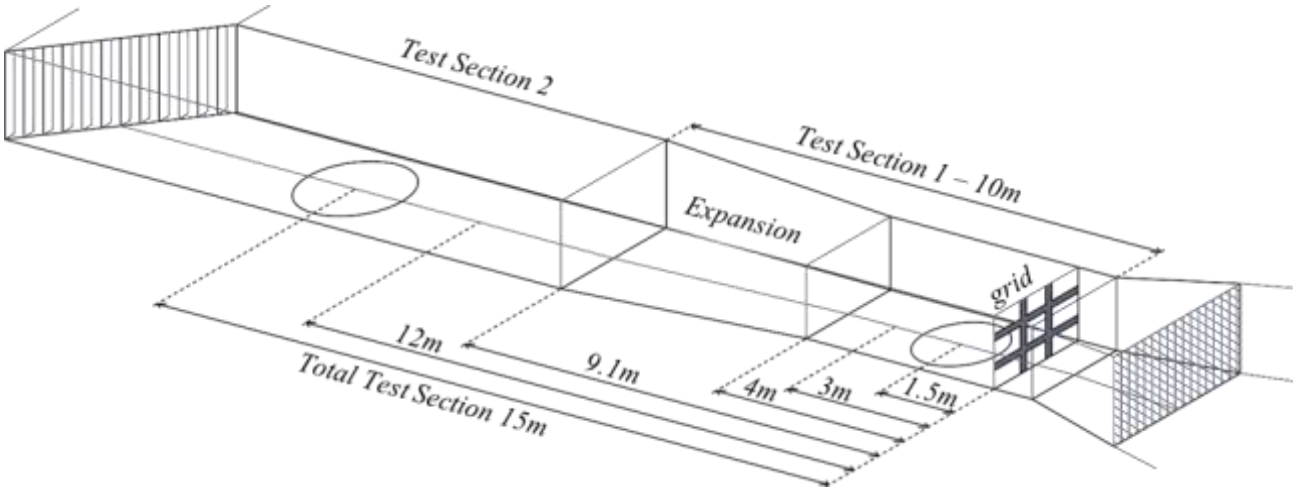

Fig. 3 – Experimental setup using the test Section 1 of the Wind Tunnel of the University of Liège.

In Fig. 4 the set of grids is exemplified. The name of the grids and their different mesh size is also represented. The velocity measurements have been performed using a Cobra probe in order to have a high-quality estimation of all velocity components, at the half-height of the tunnel $H = 1.07m$.

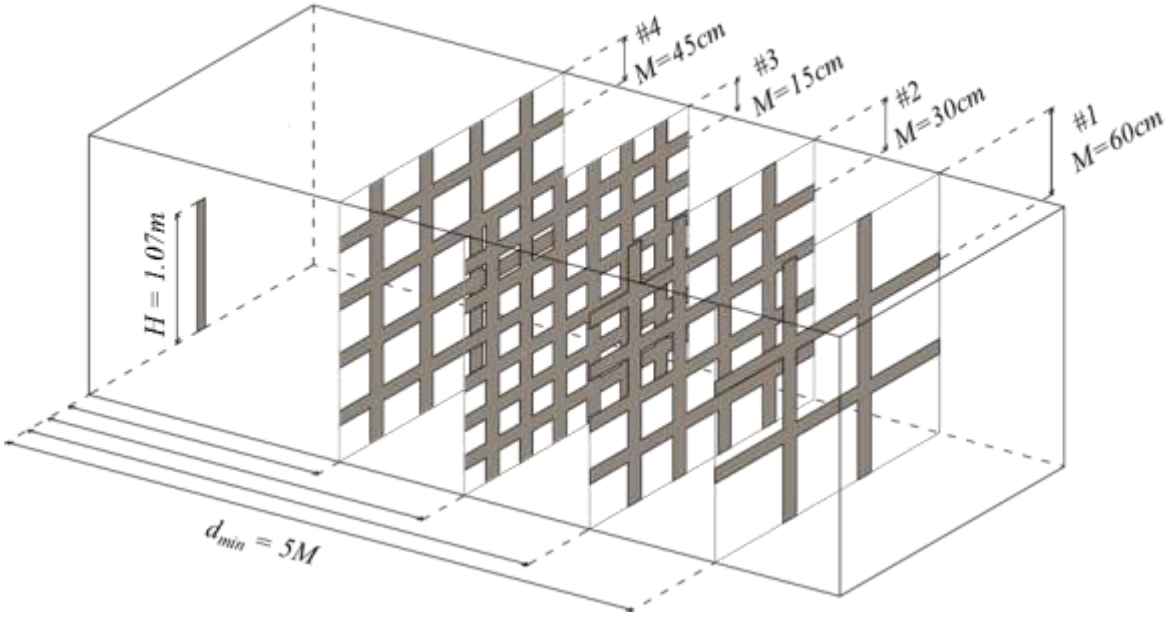

Fig. 4 – Scheme of the set of grids used in the experiment.

4. *Results*

Table 3 – Legend for results

Grid	Symbol	Rotor velocities
#1	+	5
#2	□	10
#3	○	15
#4	◇	20

Results are here briefly introduced for 4 grids, 4 velocities and 5 positions. In Table 3 a reference to the symbols used to present results in the rest of the paper is provided. Time histories of *60 s* have been recorded at *500 Hz* sampling rate using a Cobra Probe placed at the half-height of the wind tunnel section. The signals have then been post-processed to compute the longitudinal and transversal statistics: turbulence intensity, integral length scale of turbulence, Taylor's length scale of turbulence. The isotropy of the flow is also studied.

Mean velocity decay and wind tunnel contraction

Before introducing the turbulent field results, a close look at the mean velocity is given in Fig. 5 to show the effect of the expansion of the tunnel's cross-section. In fact, a steep decay of the mean velocity takes place because of the presence of an expansion (Fig. 3). While a decay is normally expected in wind tunnel testing, the expansion increases its rate. Unfortunately, this was an ineliminable feature of the wind tunnel, and therefore results need to be accordingly interpreted.

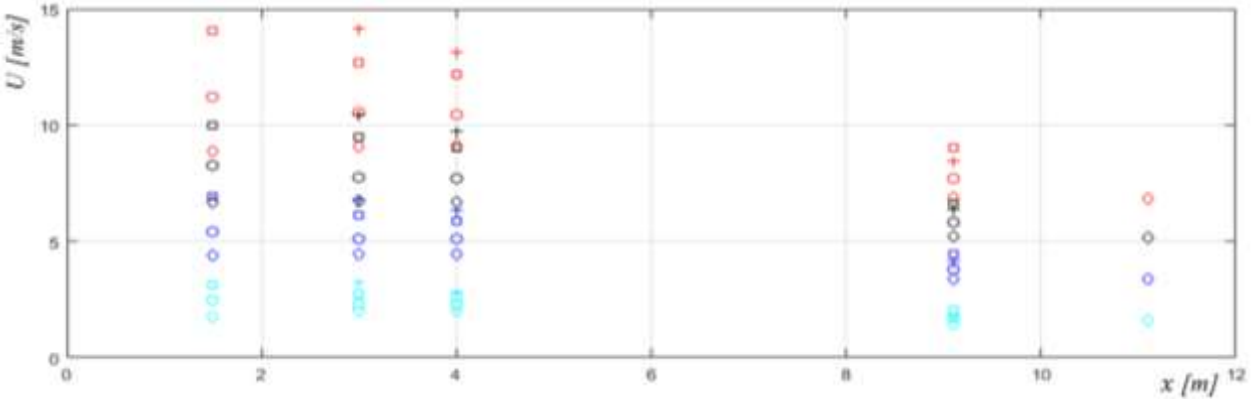

Fig. 5 – Mean Velocity plotted against distance from the grid. From 4 to 9.1m the expansion is present.

Turbulence Intensity and Integral Length Scale

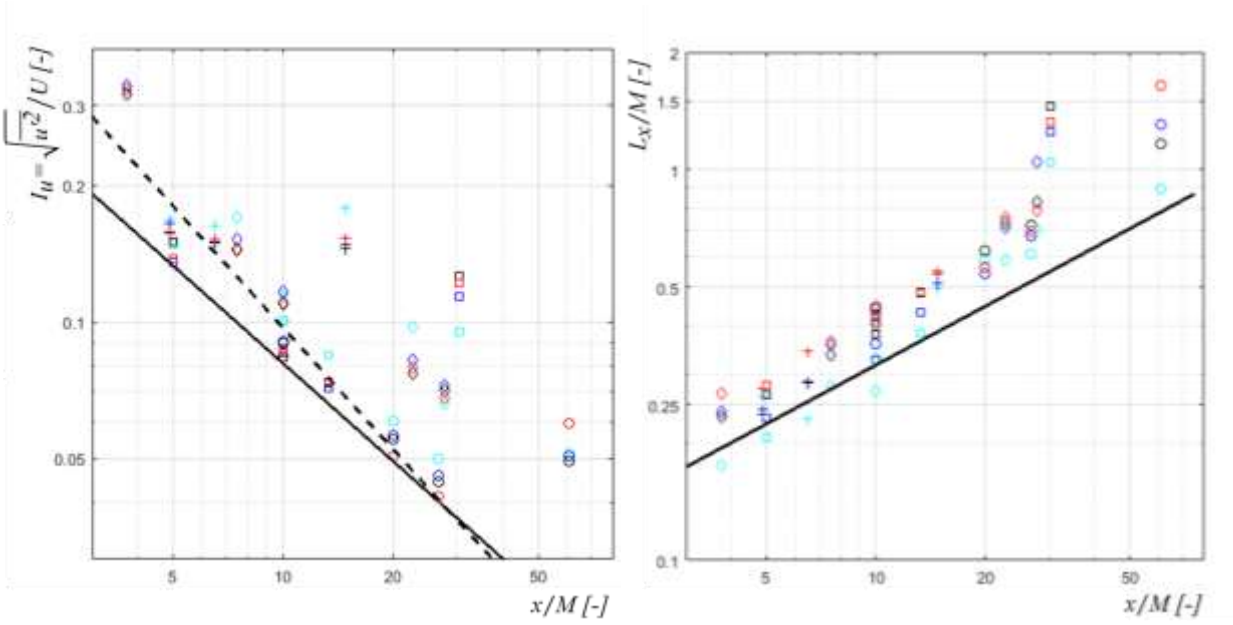

Fig. 6 – a) Turbulence Intensity and b) Integral length scale against mesh distance. Logarithmic scale.

In Fig 6 turbulence intensity and integral length scale are compared in a non-dimensional graph against mesh distance. The results are presented for all distances, grids and velocities measured. A comparison is then provided with the empirical formulas presented in Section 2.2. As it can be noticed, an apparent sparsity of the data takes place. However, looking at the dimensional plot of Fig. 7, the deviation from the empirical laws takes place downstream the expansion of the wind tunnel cross-section. This is due to the aforementioned mean velocity decay, which in turn affects the definition of turbulent statistics. Regarding the integral length scale of turbulence the empirical formulas offer a poor prediction of the actual values: a value for the empirical constant $C=0.1$ seems more likely to predict the behaviour of this specific setup.

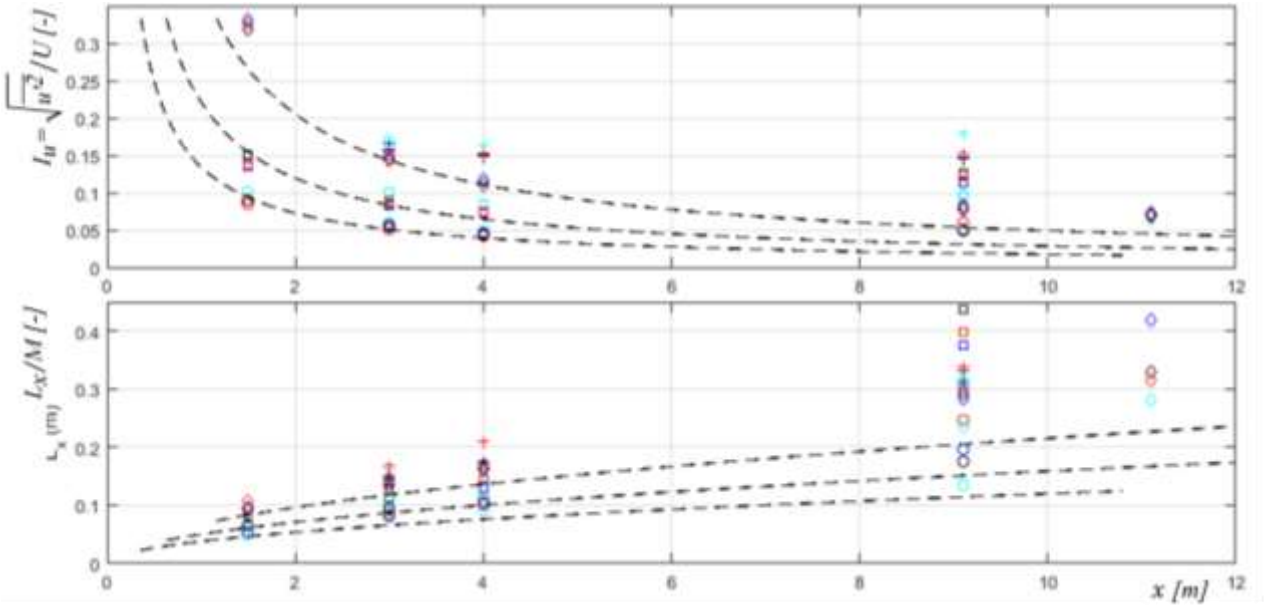

Fig. 7 – a) Turbulence Intensity and b) Integral length scale against distance from grid.

Taylor's or micro-length scale of turbulence

Most of the applications of grid turbulence do not report an assessment of Taylor's scale of turbulence, however, it gives an estimation of the importance of the viscosity in affecting the dissipation of turbulence. In this setup, the micro-scales do not change significantly with distance, being only dependent on the Reynolds number (Fig. 8). This is clear also in Fig. 8b, where the ratio between the integral and micro scales is shown as growing with lower Reynolds numbers.

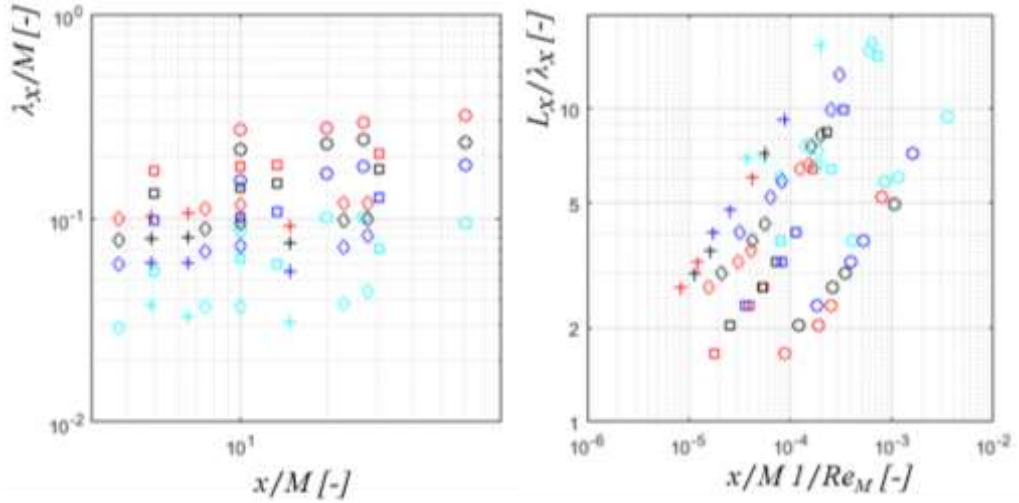

Fig. 8 – a) Taylor's or micro scale of turbulence; b) ratio between micro and integral length scale.

4.1. Isotropy

A detailed study is proposed in the following to understand the actual rate of isotropy. Together with transversal and vertical turbulence intensity also Taylor's and integral length scale are presented.

Turbulence intensity

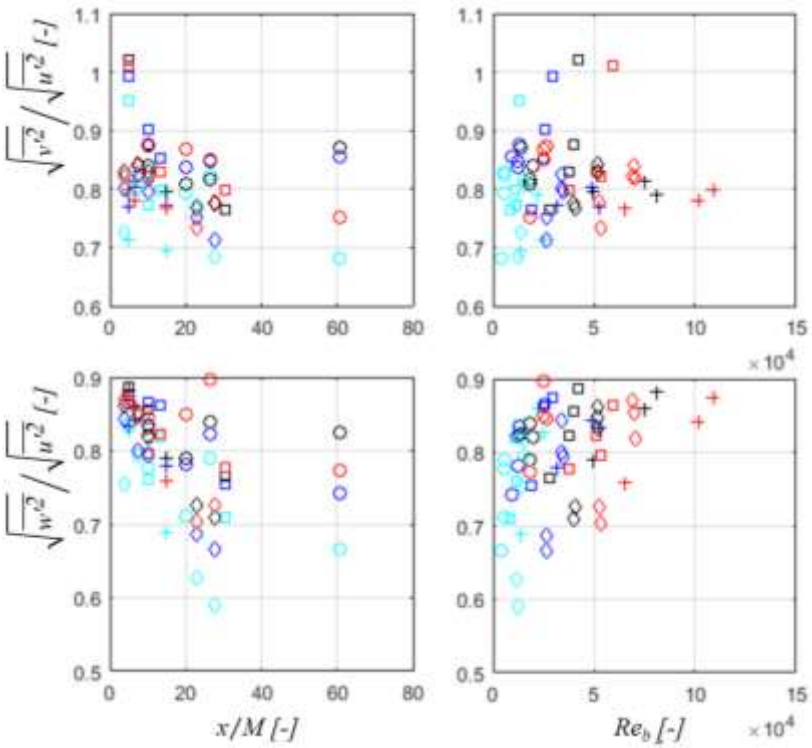

Fig. 9 – Ratio between turbulence intensities: a) mesh distance; b) bar Reynolds number

The isotropy of turbulence intensity is defined as

$$I_v/I_u = \sqrt{\overline{v'^2}} \Big/ \sqrt{\overline{u'^2}} \approx 1$$

Fig. 9 illustrates the isotropy of turbulence intensity against the mesh distance and the bar Reynolds number, defined as

$$Re_b = \bar{u}\, b/\nu$$

Fig. 9 shows as the isotropy is not strictly dependent on the distance, as moving further from the grid no significant gain in the rate of isotropy is encountered. However, isotropy shows a remarkable effect of the bar Reynolds number: the higher Re_b the more isotropic the flow. Turbulence intensity results show that isotropy reaches $\approx 80\%$ for the transversal component and $\approx 90\%$ for the vertical one, showing a broadly acceptable level of isotropy even relatively close to the grid.

Integral length scale of turbulence

As noticed for Fig. 8, also integral length scale shows to depend more on bar Reynolds number than the mesh distance.

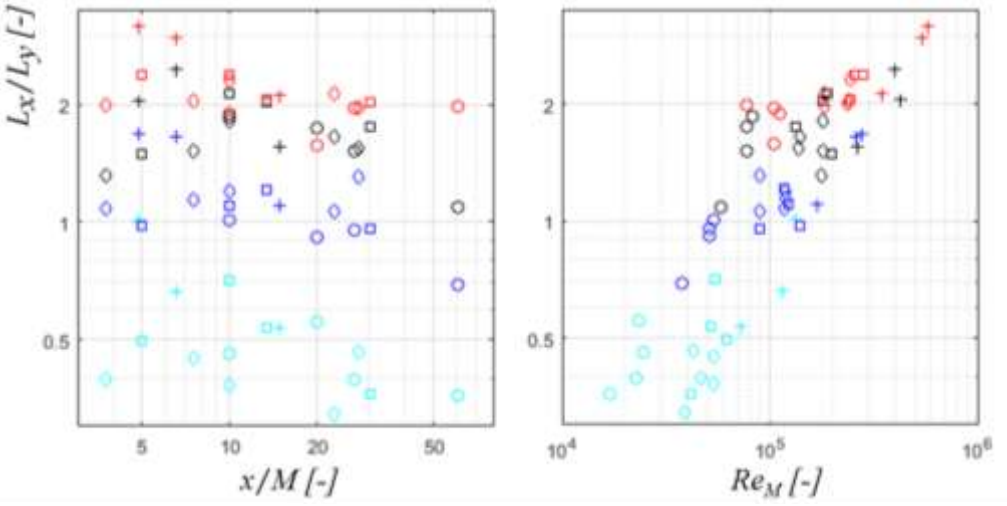

Fig. 10 – Ratio of longitudinal and transversal integral length scale of turbulence.

A closer look reveals that the isotropy condition for the integral length scale of turbulence, defined as

$$L_x/L_y = \int_0^\infty R_{uu}(\tau)d\tau \Big/ \int_0^\infty R_{vv}(\tau)d\tau \approx 2$$

Is broadly met when u_{rot}=*15-20m/s* while the lower velocities show a rather anisotropic behaviour. It is unclear, as shown in figure 9b, if the isotropy remains constant with growing velocity or continues to follow the monotonic growth behaviour.

Taylor's micro scale of turbulence

As for the integral length scales, the same conclusion can be drawn for the micro-scales: an acceptable rate of isotropy strongly depending on the Reynolds number. Here the isotropy condition is given by

$$\frac{\lambda_x}{\lambda_y} = \frac{\overline{u'^2}}{\overline{y'^2}} \frac{\int n^2 E_v \, dn}{\int n^2 E_u \, dn} \approx \sqrt{2}$$

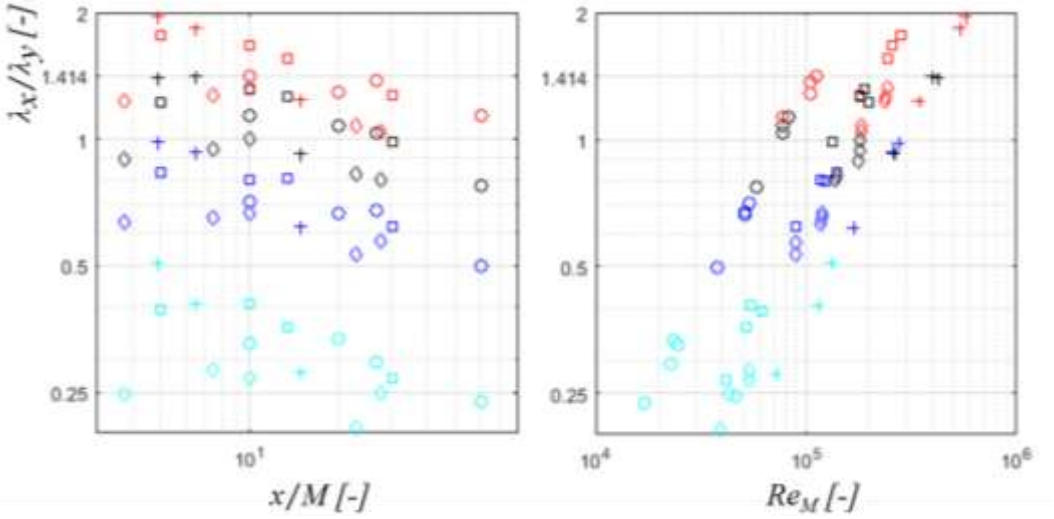

Fig. 11 – Ratio of longitudinal and transversal Taylor's length scale of turbulence.

4.2. Spectrum of turbulence

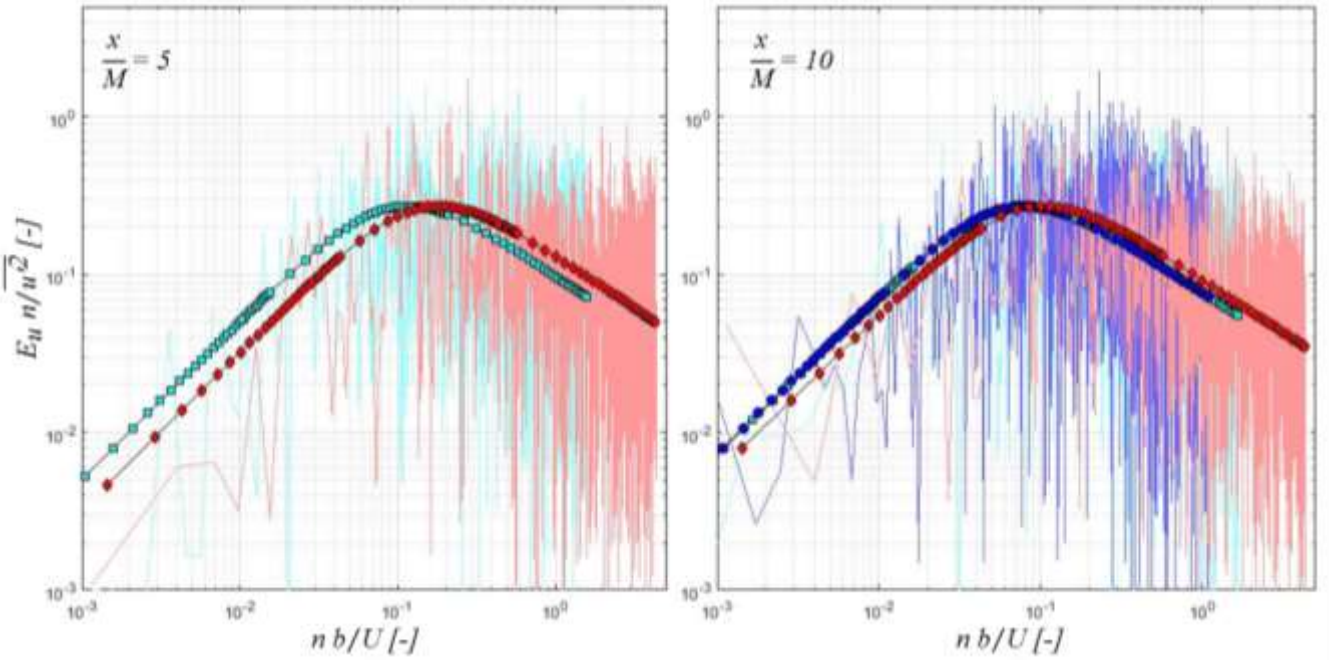

Fig. 12 – Non dimensional Spectrum of turbulence for grids #2, #3, #4 for positions a) x/M =5 and b) x/M=10.

In Fig. 12 the non-dimensional spectrum of turbulence is plotted. The spectra are computed using the FFT algorithm and then fitted with a von Karman formulation based on the definition of the integral length scale, which has been calculated using the definition of autocorrelation function. The turbulence field is sufficiently developed and broad-banded also for *x/M=5*, not showing any particular effect of the single wakes of the bars, which would have been noticeable by peaks in the spectra. Therefore, it can be concluded that the turbulence field is sufficiently developed also close to the grid measurement points.

5. Conclusions: the inlet design for future wind tunnel testing

The results show a rather isotropic flow field. Then, the resulting turbulence intensity and integral length scale can be plotted together to form a design chart to choose the needed turbulence characteristics. Being the aim to provide constant turbulence intensity with varying scale and vice versa, in Fig. 13 a plot is proposed to understand the possible configurations. The results neglect the lowest velocity $u_{rot}=5m/s$ and are fitted using a bi-exponential formulation using the least square algorithm. The use of a bi-exponential was necessary to take into account the effect of the expansion on the statistics. The graph shows multiple points of interest where integral length scales up to 33cm can be reached and turbulence intensity of 15% can be achieved.

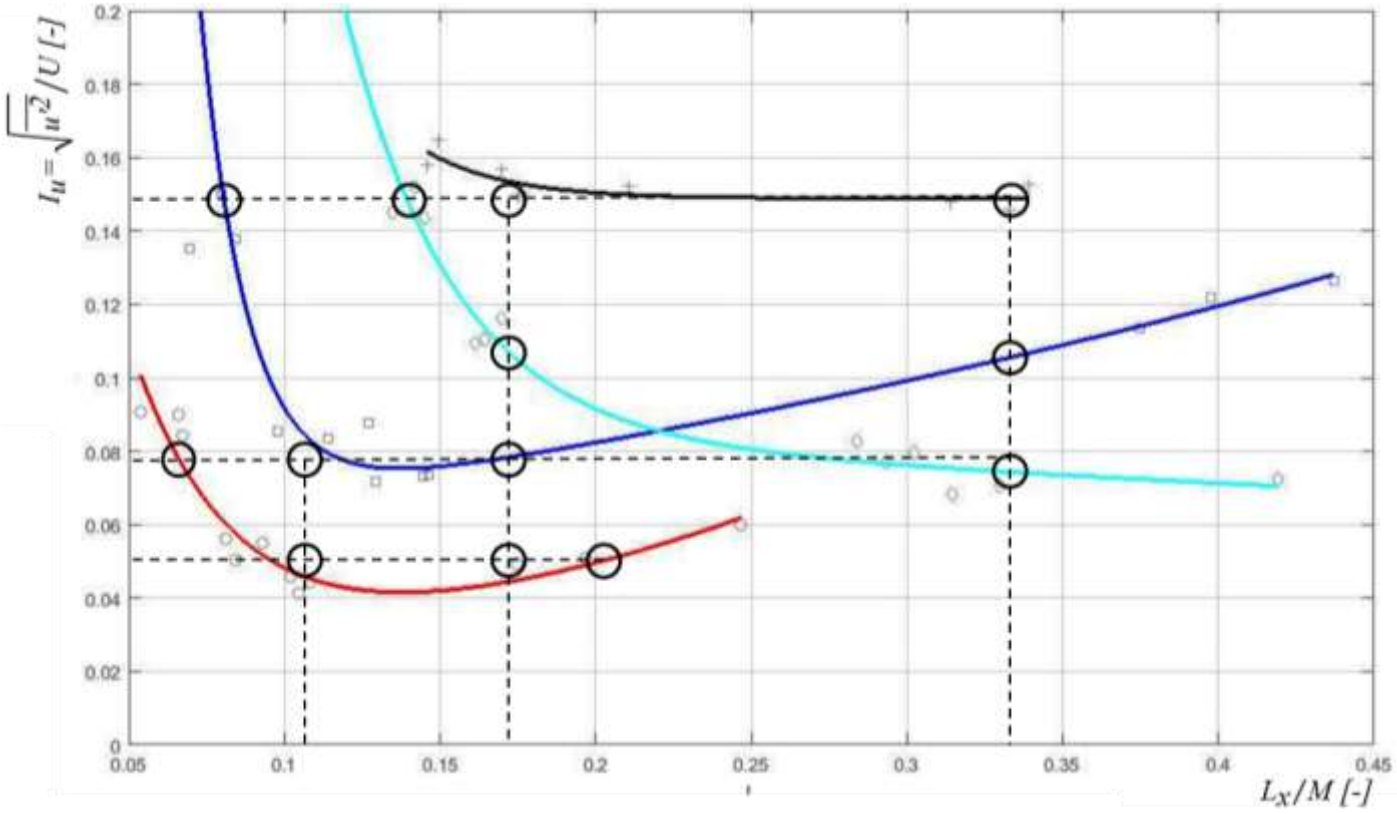

Fig. 13 – Turbulence Intensity versus Integral Length Scale of turbulence

In the next steps of the research the statistics will be studied in more details to understand the flow field to be used as an inlet for an investigation about the effect of turbulence on the aerodynamic performance of bluff bodies.

6. References

Batchelor, G.K., 1953. The Theory of Homogeneous Turbulence. Cambridge University Press.

Bearman, P.W., Morel, T., 1983. Effect of free stream turbulence on the flow around bluff bodies. Prog. Aerosp. Sci. 20, 97–123.

Bereketab, S., Wang, H.-W., Mish, P., Devenport, W.J., 2000. The Surface Pressure Response of a

NACA 0015 Airfoil Immersed in Grid Turbulence. Volume 1; Characteristics of the Turbulence.
Brzek, B., Torres-Nieves, S., Lebrón, J., Cal, R., Meneveau, C., Castillo, L., 2009. Effects of free-stream turbulence on rough surface turbulent boundary layers. J. Fluid Mech. 635, 207.
Cal, R.B., Lebrón, J., Castillo, L., Kang, H.S., Meneveau, C., 2010. Experimental study of the horizontally averaged flow structure in a model wind-turbine array boundary layer. J. Renew. Sustain. Energy 2, 13106.
Cekli, H.E., van de Water, W., 2010. Tailoring turbulence with an active grid. Exp. Fluids 49, 409–416.
Comte-Bellot, G., Corrsin, S., 1966. The use of a contraction to improve the isotropy of grid-generated turbulence. J. Fluid Mech. 25, 657.
Hinze, J.O., 1975. Turbulence. McGraw-Hill.
Kang, H.S., Chester, S., Meneveau, C., 2003. Decaying turbulence in an active-grid-generated flow and comparisons with large-eddy simulation. J. Fluid Mech. 480, 129–160.
Laneville, A., 1973. Effects of turbulence on wind induced vibrations of bluff cylinders.
Laneville, A., 1990. Turbulence and blockage effects on two dimensional rectangular cylinders. J. Wind Eng. Ind. Aerodyn. 33, 11–20.
Laneville, A., Gartshore, I., Parkinson, G., 1975. An explanation of some effects of turbulence on bluff bodies. … Fourth Int. Conf. Wind ….
Lee, B.E., 1975. Some effects of turbulence scale on the mean forces on a bluff body. J. Wind Eng. Ind. Aerodyn. 1, 361–370.
Makita, H., 1991. Realization of a large-scale turbulence field in a small wind tunnel. Fluid Dyn. Res. 8, 53–64.
Makita, H., Sassa, K., 1991. Active Turbulence Generation in a Laboratory Wind Tunnel. In: Johansson, A. V, Alfredsson, P.H. (Eds.), Advances in Turbulence 3: Proceedings of the Third European Turbulence Conference Stockholm, July 3--6, 1990. Springer Berlin Heidelberg, Berlin, Heidelberg, pp. 497–505.
Maldonado, V., Castillo, L., Thormann, A., Meneveau, C., 2015. The role of free stream turbulence with large integral scale on the aerodynamic performance of an experimental low Reynolds number S809 wind turbine blade. J. Wind Eng. Ind. Aerodyn. 142, 246–257.
Mannini, C., Marra, A.M., Pigolotti, L., Bartoli, G., 2017. The effects of free-stream turbulence and angle of attack on the aerodynamics of a cylinder with rectangular 5:1 cross section. J. Wind Eng. Ind. Aerodyn. 161, 42–58.
MCLAREN, F.G., SHERRATT, A.F.C., MORTON, A.S., 1969. Effect of Free Stream Turbulence on the Drag Coefficient of Bluff Sharp-edged Cylinders. Nature 223, 828–829.
Mish, P.F., Devenport, W.J., 2006. An experimental investigation of unsteady surface pressure on an airfoil in turbulence—Part 1: Effects of mean loading. J. Sound Vib. 296, 417–446.
MULHEARN, P.J., 1973. Stagnation and Reattachment Lines on a Cylinder of Square Cross-section in Smooth and Turbulent Flows. Nature, Publ. online 26 Febr. 1973; | doi10.1038/10.1038/physci241165a0 241, 165.
Mydlarski, L., Warhaft, Z., 2006. On the onset of high-Reynolds-number grid-generated wind tunnel turbulence. J. Fluid Mech. 320, 331.
Nakamura, Y., 1993. Bluff-body aerodynamics and turbulence. J. Wind Eng. Ind. Aerodyn. 49, 65–78.
Nakamura, Y., Ohya, Y., Ozono, S., 1988. The effects of turbulence on bluff-body mean flow. J. Wind Eng. Ind. Aerodyn. 28, 251–259.
Roach, P.E., 1987. The generation of nearly isotropic turbulence by means of grids. Int. J. Heat Fluid Flow 8, 82–92.
Sicot, C., Devinant, P., Loyer, S., Hureau, J., 2008. Rotational and turbulence effects on a wind turbine blade. Investigation of the stall mechanisms. J. Wind Eng. Ind. Aerodyn. 96, 1320–1331.
Swalwell, K., Sheridan, J., Melbourne, W., 2004. The effect of turbulence intensity on performance of a NACA 4421 airfoil section. 42nd AIAA Aerosp.
Swalwell, K.E., 2005. The effect of turbulence on stall of horizontal axis wind turbines 1–307.
Wang, S., Zhou, Y., Alam, M.M., Yang, H., 2014. Turbulent intensity and Reynolds number effects on an airfoil at low Reynolds numbers. Phys. Fluids 26, 115107.